Proceedings of the 9th World Congress on Mechanical, Chemical, and Material Engineering (MCM'23)
Brunel University, London, United Kingdom - August 06-08, 2023
Paper No. ICMIE 147
DOI: 10.11159/icmie23.147

Virtual Testing of Synthetic Polycrystal Microstructures Predicting Elastic Properties of Additive Manufactured Alloy 718

Liene Zaikovska[1], Magnus Ekh[1], Chamara Kumara[1]
[1]Department of Engineering Science, University West
Gustava Melins Gata 2, 46132 Trollhättan, Sweden
liene.zaikovska@hv.se; magnus.ekh@hv.se; chamara.kumara@hv.se

Abstract - Additive manufacturing (AM) is gaining significant attention in manufacturing engineering owing to its advantages compared to traditional manufacturing methods. Microstructures that result from the AM process often lead to anisotropic mechanical properties of produced components. In this study the Ni-based Alloy 718 is analysed. It has been shown that the microstructure of this polycrystalline material can be tailored to obtain different grain morphology distributions and crystallographic textures. In this paper, the reproduction of three typical microstructures, equiaxed, columnar and combined (equiaxed and columnar), are investigated to determine their elastic anisotropic properties. Virtual testing is applied on synthetic representative volume elements (RVE) for the equiaxed and columnar grain structures, and representative area element (RAE) for the combined structure. The crystal elasticity finite element method (CEFEM) is utilized to predict macroscopic elastic properties. This method allows the implementation of grain crystallographic orientations as input texture and the generation of homogenized elastic stiffness matrix predicting the directional engineering stresses of polycrystal microstructures. The comparison of the simulation results for the three microstructures studied demonstrates significant property variation. Also, the comparison of the different number of grains and various interface area cases of the combined structure shows diversity in the results presented in this study.

***Keywords*:** additive manufacturing, polycrystal, crystal elasticity finite element, cohesive zone, homogenization, anisotropy

1. Introduction

Additive manufacturing (AM), also known as 3D printing of metals, is a process in which metal parts are built layer by layer using computer-controlled e.g., laser or electron beam to melt and fuse metal powder or wire. There are several different AM technologies for metals, including powder bed fusion, directed energy deposition, binder jetting, and sheet lamination. AM offers several advantages including unique geometries, improved performance, reduced weight, and increased efficiency.

One advantage of metal AM process is that it is capable of manufacturing complex-shaped metal components with good properties for structural and mechanical applications. By varying process parameters, the different microstructures can be achieved which results in different mechanical properties. The subsequent heat treatments will also initiate changes in microstructure and hence mechanical properties. Elastic properties of AM parts can vary significantly depending on the orientation of the build direction with respect to the loading direction [1].

The Alloy 718 is used in this study. Also this material's texture is strongly influenced by process parameters and affected by changes in processing setup which makes it difficult to establish a conclusive picture of the process-microstructure correlations [2]. Alloy 718 is a precipitation hardened nickel-based superalloy which can be found in gas turbines, nuclear reactors, and spacecraft structural components [3]. This alloy is widely used due to its high strength at moderate temperatures, corrosion and oxidation resistance, and its creep and fatigue resistance properties [4]. The nickel-based superalloys at the grain level typically introduce anisotropic elastic material behaviour which strongly depends on the grain orientation. When the microstructure contains textured grains found e.g., in AM built components [5], cold rolled sheets [6], single crystal superalloys [7], it will lead to anisotropic material behaviour. As a result, the Young's modulus, shear modulus and Poisson's ratio will depend on the sample angle with respect to the build direction [8].

Since polycrystalline materials at microscale deform heterogeneously, the representative volume element (RVE) method can be used to simulate the behaviour of a material at the microscale and to model the material response when subjected to various loading conditions [9], [10]. There are several tools and methods that can be used for generating RVEs such as image

processing application, e.g. the electron backscatter diffraction (EBSD) [11], [12], three dimensional scans produced by synchrotron X-ray diffraction [13] or MTEX [14] and Voronoi tessellation representing the individual grains or phases of the microstructure as the basis for an RVE which is commonly used in e.g., Neper [15], Dream3D [16]. When modelling the transition zone between regions with e.g., equiaxed and columnar grains, a cohesive zone is created as a representative area element (RAE). Applying RAE method, it is possible to identify the local stress response and the elastic stiffness response within the transition area.

The most common and simplest way to implement the homogenization of polycrystals is to apply Taylor model (also named Voigt or Iso-strain) or Reuss model (also called Iso-stress) [17], [18], [19], [20], [21] integrated in the computational scripts such as MATLAB [22], MTEX [14]. Another, more detailed homogenization technique for metallic materials is the physics-based crystal plasticity finite element (CPFE) modelling [23], [24], [25]. CPFE is a computational technique that models the deformation behaviour of polycrystalline materials by simulating the behaviour within individual crystals. CPFE has been used to study the effects of grain size, grain boundary structure, and crystallographic texture on the mechanical behaviour of metals and alloys. By applying the CPFE method, it is possible to compute the yield strength, ultimate tensile strength, elongation at failure and micro-hardness [26]. In [27] by using CPFE it was shown that the grain size as well as grain morphology affect mechanical properties such as yield strength and the initial strain hardening modulus of AM 316L stainless steel. Similarly, another study [28] done on Al 7075-T6 microstructure models with different textures, grain sizes, and grain morphologies showed an influence on the yield strength. Here it was highlighted that the yield strength is sensitive to the change of grain aspect ratio. Additionally, the importance of the grain size distribution is highlighted in the context. The simulation results demonstrated that the grain size and morphological effects influence the fatigue response. The equiaxed grains exhibited the highest force against fatigue crack formation while the elongated grain shapes might lead to an extreme change in fatigue response showing the importance of grain morphology in fatigue analysis. Likewise, studying the Hastelloy-X material and selective laser melting (SLM) process in [29] showed that the microstructure texture made a clear influence on the elastic and plastic behaviours in terms of the yield point and elastic modulus.

Crystal elasticity finite element (CEFE) is a part of CPFE computational technique that model only the elastic behaviour of single crystals. In many industrial applications, the component design is such that the material is in its elastic regime. In such cases, the elastic stiffness is the main contributor to the performance of the materials. Due to grain morphology and texture in the AM built component the macroscopic elasticity might become anisotropic. When investigating the transition zone of the combined structures, it is important to identify the local stress field [30]. To capture the local stress field would be very difficult or even impossible employing analytical methods. Thereby the CPFE/CEFE modelling tool can be used for prediction of this type of material behaviour [31]. Since there is no research done on mechanical properties of a cohesive zone model representing the transition area in combined AM microstructures, with this contribution we will investigate numerical modelling of three different microstructures, equiaxed, columnar and combined (equiaxed and columnar). In particular, we will investigate how many grains that are needed in a volume element to get a representative elastic response as well as the resulting elastic behaviour of the representative volume and area element.

2. Methodology

In this study, the software Neper is applied to generate RVE/RAEs. Neper is also used to mesh (finite element discretize) the resulting complex geometries, and to visualize microstructure properties using Inverse Pole Figure (IPF) and Pole Figure (PF) maps. The generated mesh-files are adapted for further calculations in finite element software such as ABAQUS [32]. In all synthetic AM microstructures presented in this study, the sample direction is assumed parallel to building direction. The grains of the microstructures are assumed to be equiaxed and columnar, as well as their combination. These are obtained by using different Voronoi diagrams in Neper. Tetrahedral second order element meshes are generated with approximately 200 000 elements for the equiaxed and columnar cases, and 700 000 elements for the combined grain structure cases. For the RAE homogenizations, 2D area sections of approximately 20-40 000 elements were used. Cubic symmetric linear elasticity of the grains was implemented with following elastic single crystal constants found in literature [33], $C_{11} = 259.5$ [GPa], $C_{12} = 179.0$ [GPa], $C_{44} = 109.6$ [GPa].

2.1. Representative Volume Element (RVE) Generation

The equiaxed microstructure is built using random crystallographic orientations of the grains to study the resulting macroscopic isotropic elasticity. In the case of columnar grain structures, the number of grains as well as the influence of the aspect ratios are studied. The crystallographic orientations are chosen with strong texture along the building direction, i.e., the Z-axis. This columnar texture is used to study the resulting macroscopic transversal isotropy. In the equiaxed cases, number of grains containing 200, 500, 1000 and 1500 are implemented. In the columnar cases, number of grains containing 50, 100, 200 and 1500 as well as aspect ratios of 3, 5 and 10 are also studied. In addition, the chosen crystallographic directions are also studied using PF and IPF maps.

2.2. Representative Area Element (RAE) generation

Combined microstructure is often characterized by the presence of different types of microstructures within a single part, including equiaxed grains and columnar grains.

In this study, three different cases were investigated where equiaxed grains are combined with the columnar grains, and 2D area element as the interface of the transition zone, is analysed. The transition interface TI(H) = 0.15mm was specified during the tessellation stage. In this study three cases of different heights of the RAE cohesive zone are analysed to compare the impact of the chosen zone heights and interface grain shapes shown in Fig.1. The RAE method is used to identify the homogenized stiffness responses within the region between two structures.

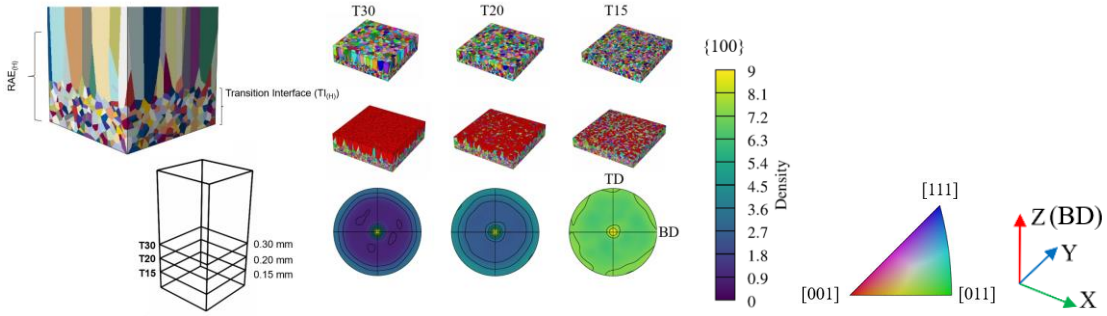

Fig. 1: Schematic representation of the representative area element height ($RAE_{(H)}$), positions used in the three studied cases (T30, T20, T15) of cohesive zone homogenization and combined microstructure models including the pole figures representing initial crystallographic texture cases used in the RAE cohesive zone study.

2.3. Computational Homogenization

The homogenized properties can be determined by the computation of mechanical response of an RVE [26]. The Voigt (Iso-strain) and Reuss (Iso-stress) approximations are the simplest homogenization approaches. In the case of the Voigt approximation, the strain is assumed equal for all grains during the deformation and in the case of the Reuss approximation, the stress applied to all grains is assumed to be equal. Hence the effective properties of the RVE for the Voigt and Reuss approximations are obtained presented in Eqs. (1) - (2) where V is the total volume of the polycrystal body, V_{n} denotes the volume of the grain n and $\mathbb{E}_{\mathrm{n}}$ represents the stiffness within the grain n.

$$\overline{\mathbb{E}}_{Voigt} = \frac{1}{V}\sum_{\mathrm{n}=1}^{\mathrm{n}_{\mathrm{grain}}} V_{\mathrm{n}}\,\mathbb{E}_{\mathrm{n}}\; with\; V = \sum_{\mathrm{n}=1}^{\mathrm{n}_{grain}} V_{\mathrm{n}} \tag{1}$$

$$\overline{\mathbb{E}}_{Reuss} = \left(\frac{1}{V}\sum_{\mathrm{n}=1}^{\mathrm{n}_{\mathrm{grain}}} V_{\mathrm{n}}\,{\mathbb{E}_{\mathrm{n}}}^{-1}\right)^{-1} with\, V = \sum_{\mathrm{n}=1}^{\mathrm{n}_{grain}} V_{\mathrm{n}} \tag{2}$$

To include the influence of grain morphology, the equilibrium equations for the complete RVE and RAE, described in the previous section, are solved with the FE-method. To find the macroscopic elastic stiffness $\bar{E}$ that describes the relation between the homogenized macroscopic stress $\bar{\sigma}$ and strain $\bar{\varepsilon}$ the virtual testing is used. In Voigt form the macroscopic elastic relation can be written as follows:

$$\begin{bmatrix}\bar{\sigma}_{11}\\ \bar{\sigma}_{22}\\ \bar{\sigma}_{33}\\ \bar{\sigma}_{12}\\ \bar{\sigma}_{13}\\ \bar{\sigma}_{23}\end{bmatrix}=\begin{bmatrix}\bar{\bar{E}}_{1111} & \bar{\bar{E}}_{1122} & \bar{\bar{E}}_{1133} & \bar{\bar{E}}_{1112} & \bar{\bar{E}}_{1123} & \bar{\bar{E}}_{1131}\\ \bar{\bar{E}}_{2211} & \bar{\bar{E}}_{2222} & \bar{\bar{E}}_{2233} & \bar{\bar{E}}_{2212} & \bar{\bar{E}}_{2223} & \bar{\bar{E}}_{2213}\\ \bar{\bar{E}}_{3311} & \bar{\bar{E}}_{3322} & \bar{\bar{E}}_{3333} & \bar{\bar{E}}_{3312} & \bar{\bar{E}}_{3323} & \bar{\bar{E}}_{3313}\\ \bar{\bar{E}}_{1211} & \bar{\bar{E}}_{1222} & \bar{\bar{E}}_{1233} & \bar{\bar{E}}_{1212} & \bar{\bar{E}}_{1223} & \bar{\bar{E}}_{1213}\\ \bar{\bar{E}}_{2311} & \bar{\bar{E}}_{2322} & \bar{\bar{E}}_{2333} & \bar{\bar{E}}_{2312} & \bar{\bar{E}}_{2323} & \bar{\bar{E}}_{2313}\\ \bar{\bar{E}}_{1311} & \bar{\bar{E}}_{1322} & \bar{\bar{E}}_{1333} & \bar{\bar{E}}_{1312} & \bar{\bar{E}}_{1323} & \bar{\bar{E}}_{1313}\end{bmatrix}\begin{bmatrix}\bar{\varepsilon}_{11}\\ \bar{\varepsilon}_{22}\\ \bar{\varepsilon}_{33}\\ 2\bar{\varepsilon}_{12}\\ 2\bar{\varepsilon}_{13}\\ 2\bar{\varepsilon}_{23}\end{bmatrix} \tag{3}$$

By virtual testing we prescribe one macroscopic strain component at a time and then the computed homogenized stress gives a column in the stiffness matrix. In practise, this is done by prescribing the displacement vector u on the boundary Γ of the volume element V governing field equations at the point x as follows:

$$\mathrm{u} = \overline{\mathbf{H}}\,\mathrm{x} \tag{4}$$

where $\overline{\mathrm{H}}$ is the macroscopic displacement gradient. The strain components are obtained from the components of $\overline{\mathrm{H}}$ as:

$$\bar{\varepsilon}_{11} = \bar{\boldsymbol{H}}_{11}, \bar{\varepsilon}_{22} = \bar{\boldsymbol{H}}_{22}, \bar{\varepsilon}_{33} = \bar{\boldsymbol{H}}_{33}, 2\bar{\varepsilon}_{12} = \bar{\boldsymbol{H}}_{12} + \bar{\boldsymbol{H}}_{21}, 2\bar{\varepsilon}_{23} = \bar{\boldsymbol{H}}_{23} + \bar{\boldsymbol{H}}_{32}, 2\bar{\varepsilon}_{13} = \bar{\boldsymbol{H}}_{13} + \bar{\boldsymbol{H}}_{31} \tag{5}$$

which is a result from the following relation:

$$\bar{\boldsymbol{\varepsilon}} = (\bar{\boldsymbol{H}} + \bar{\boldsymbol{H}}^{T})/2 \tag{6}$$

The choice to prescribe the displacement linearly according to $\mathrm{u} = \overline{\mathbf{H}}\,\mathrm{x}$ on Γ is one convenient alternative when using the FEM. Other choices are available in literature such as to prescribe the traction (Neumann boundary conditions) or to apply periodic boundary conditions.

The homogenized stress $\bar{\boldsymbol{\sigma}}$ can now be computed from the FE analysis as:

$$\bar{\boldsymbol{\sigma}} = \frac{1}{V}\sum_{e=1}^{n_{elem}} V_e\,\boldsymbol{\sigma_e} \tag{7}$$

where V_e is the element volume and $\boldsymbol{\sigma_e}$ is the average stress in the element, so called centroid.

In the case of combined structure, the Cohesive law, representing the effective properties of the transition region, can be written denoted in Eq. (8) where t_n, t_s, t_t represents the normal and shear tractions defined by the stiffness matrix K_{ij} multiplied by the normal and shear strains.

$$\begin{bmatrix}t_n\\ t_s\\ t_t\end{bmatrix} = \begin{bmatrix}K_{nn} & K_{ns} & K_{nt}\\ K_{sn} & K_{ss} & K_{st}\\ K_{tn} & K_{ts} & K_{tt}\end{bmatrix}\begin{bmatrix}\varepsilon_n\\ \varepsilon_s\\ \varepsilon_t\end{bmatrix} \tag{8}$$

The normal and shear strains are computed from the displacement u_n^+ and u_n^- jumps between opposite site of the volume as:

$$\varepsilon_n = [u_n]/RAE_H = (u_n^+ - u_n^-)/RAE_H, \varepsilon_s = [u_s]/RAE_H = (u_s^+ - u_s^-)/RAE_H, \\ \varepsilon_t = [u_t]/RAE_H = (u_t^+ - u_t^-)/RAE_H \tag{9}$$

where RAE_H is corresponding distance between the opposite sides. The normal and shear tractions are computed as:

$$t_n = \bar{\boldsymbol{\sigma}}\colon(\mathbf{n}\otimes\mathbf{n}), t_s = \bar{\boldsymbol{\sigma}}\colon(\mathbf{n}\otimes\mathbf{s}), t_t = \bar{\boldsymbol{\sigma}}\colon(\mathbf{n}\otimes\boldsymbol{t}) \tag{10}$$

where **n**, **s**, $\boldsymbol{t}$ are unit-length normal and shear directions respectively.

If prescribing $u_n^+ \neq 0$, $u_s^+ = u_t^+ = 0$, it will give the following strain:

$$\varepsilon_n = (u_n^+ - 0)/RAE_H = u_n^+/RAE_H,, \varepsilon_s = \varepsilon_t = 0 \tag{11}$$

whereby K_{nn}, K_{sn}, K_{tn} can be computed from the volume averaged stress $\bar{\boldsymbol{\sigma}}$ using Eq. (6) as follows:

$$K_{nn} = t_n/\varepsilon_n = \bar{\boldsymbol{\sigma}}\colon(\mathbf{n}\otimes\mathbf{n})/\varepsilon_n, K_{sn} = t_s/\varepsilon_n = \bar{\boldsymbol{\sigma}}\colon(\mathbf{n}\otimes\mathbf{s})/\varepsilon_n, K_{tn} = t_t/\varepsilon_n = \bar{\boldsymbol{\sigma}}\colon(\mathbf{n}\otimes\boldsymbol{t})/\varepsilon_n \tag{12}$$

Similar procedures are done for ε_s and ε_t to find the corresponding column in the stiffness matrix of the cohesive element.

2.4. Constitutive Model of the Grains

The crystal structure of the matrix γ phase in Alloy 718 is Face-Centred Cubic (FCC). This motivates the use of cubic cubic symmetry of the elasticity for the grains. Cubic symmetry is obtained as the special case of orthotropy (or tetragonal tetragonal symmetry) where all the principal material directions and planes are equivalent. As a result, the elastic stiffness stiffness $\mathbb{E}^e$ takes following form:

$$\mathbb{E}^e = L \, \square\otimes\square + 2G\mathbf{A_i} + [L' - L]\sum_{i=1}^{3} \boldsymbol{A}_i \otimes \boldsymbol{A}_i \tag{13}$$

where $L' = M - 2G$ and M, L, G are material elastic constants. $\square$ is the second order tensor and $\mathbf{A_i}$ is the fourth order tensor and $\boldsymbol{A}_\mathrm{i}$ are the structural tensors defined from the material directions. The three orthogonal material directions $\boldsymbol{a}_i$ define the corresponding structural tensors as follows:

$$\boldsymbol{A}_i = \boldsymbol{a}_i \otimes \boldsymbol{a}_i \; (for \; i = 1,2,3) \tag{14}$$

For the special case that the material's directions coincide with the coordinate axes, the stiffness relation for a more general case of orthotropy corresponds to:

$$\begin{bmatrix}\sigma_{11}\\ \sigma_{22}\\ \sigma_{33}\\ \tau_{12}\\ \tau_{13}\\ \tau_{23}\end{bmatrix} = \begin{bmatrix} C_{11} & C_{12} & C_{13} & 0 & 0 & 0 \\ C_{12} & C_{22} & C_{23} & 0 & 0 & 0 \\ C_{13} & C_{23} & C_{33} & 0 & 0 & 0 \\ 0 & 0 & 0 & C_{44} & 0 & 0 \\ 0 & 0 & 0 & 0 & C_{55} & 0 \\ 0 & 0 & 0 & 0 & 0 & C_{66} \end{bmatrix} \begin{bmatrix}\varepsilon_{11}\\ \varepsilon_{22}\\ \varepsilon_{33}\\ \gamma_{12}\\ \gamma_{13}\\ \gamma_{23}\end{bmatrix} \tag{15}$$

where $\sigma_{ij}, \tau_{ij}, \varepsilon_{ij}, \gamma_{ij}$ are the normal stress, shearing stress, the corresponding normal and shearing strain respectively. C_{11}, C_{22}, C_{33}, C_{12}, C_{13}, C_{23}, C_{44}, C_{55}, C_{66} are the 9 elastic constants. When analysing the homogenized elasticity for equiaxed and columnar grains, we will refer to elastic isotropy and transversal isotropy [34]. The direction vectors of each grain $\boldsymbol{a}_i$ can be expressed in terms of the Bunge angles φ_1, φ_2, φ_3. The components of these vectors in the coordinate system can be expressed as follows:

$$[\boldsymbol{a}_1] = \begin{bmatrix} cos(\varphi_1)cos(\varphi_3) - sin(\varphi_1)sin(\varphi_3)cos(\varphi_2) \\ -cos(\varphi_1)sin(\varphi_3) - sin(\varphi_1)cos(\varphi_3)cos(\varphi_2) \\ sin(\varphi_1)sin(\varphi_2) \end{bmatrix},$$
$$[\boldsymbol{a}_2] = \begin{bmatrix} sin(\varphi_1)cos(\varphi_3) + cos(\varphi_1)sin(\varphi_3)cos(\varphi_2) \\ -sin(\varphi_1)sin(\varphi_3) + cos(\varphi_1)cos(\varphi_3)cos(\varphi_2) \\ -cos(\varphi_1)sin(\varphi_2) \end{bmatrix}, [\boldsymbol{a}_3] = \begin{bmatrix} sin(\varphi_3)sin(\varphi_2) \\ cos(\varphi_3)sin(\varphi_2) \\ cos(\varphi_2) \end{bmatrix} \tag{16}$$

3. Results and Discussions

3.1. Equiaxed Microstructure

For the equiaxed microstructure, between 200-1500 grains were studied. Since this microstructure has random grain orientations and morphology, the properties should become equal in all directions. For 200 grains the results did not show complete isotropy and averaged Young's modulus for this case became 203 [GPa] while for the cases of 500, 1000 and 1500 grains, it resulted in 211 [GPa], 209 [GPa] and 210 [GPa] respectively. The average shear modulus for the 200 grains case became 80 [GPa], while for 1500 grains it became 78 [GPa]. It can be concluded that 200 grains or less would not be statistically representative, and more than 200 grains are necessary to get representative response. The Voigt and Reuss approximations were computed using MTEX where Euler-Bunge angles and grain volumes were used as input and tested for 1500 grains case. The Voigt and Reuss approximations give average Young's modulus of 217 [GPa] and 176 [GPa]

respectively. It can also be noticed that CEFE results appear much closer to the Voigt than the Reuss approximation. Voigt and Reuss models assume different types of interactions between the individual grains within the material which for Voigt will lead to a stiffer response than the Reuss model. Regarding shear modulus the results were 82 [GPa] and 65 [GPa] for the Voigt and Reuss cases respectively. The overall summary of the results can also be seen in Fig. 2.

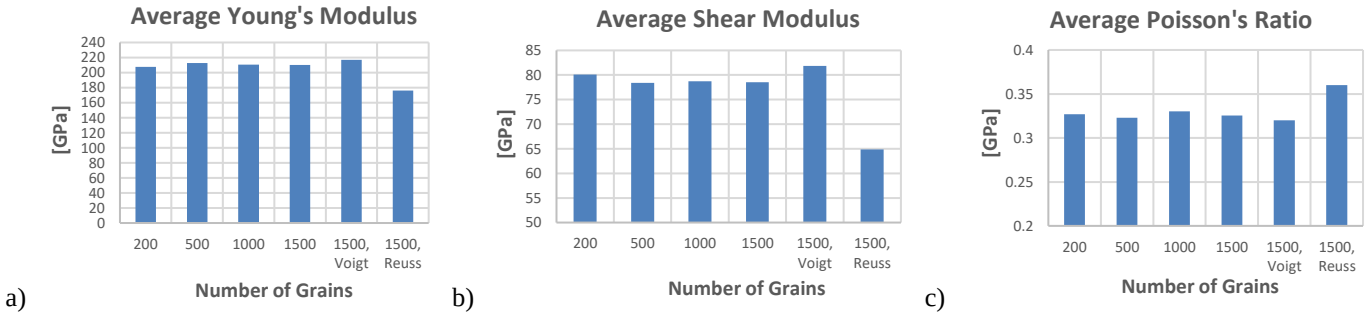

Fig. 2: Averaged a) Young's modulus, b) shear modulus and c) Poisson's ratio comparison summary.

3.2. Columnar Microstructure

For the columnar microstructure, results from 50, 100, 200 and 1500 grains as well as aspect ratios of 3, 5 and 10 were studied. The crystallographic orientations in the models in Z-direction (build direction) were set parallel to <001> direction and randomly oriented in the normal to the build direction. It can be observed from the results that there are no significant differences neither for the different number of grains, nor for the different aspect ratios. The Young's modulus in the normal to build direction becomes 163 [GPa] and parallel to build direction 113.5 [GPa]. The shear modulus in XY-plane is 65-75 [GPa] and out of the plane 110 [GPa]. Poisson's ratio becomes 0.14-0.17 in the XY-plane and 0.4 out of the plane. Similarly, as it was presented for equiaxed cases, the Voigt and Reuss results are upper and lower bounds of the columnar microstructure with 1500 grains. This behaviour can be observed for all studied properties, see Fig.3. It can also be noticed that the stiffness in normal direction of the build direction is much lower for columnar cases compared to the equiaxed cases. The stiffness in the normal direction to the AM build direction is typically much lower for columnar than for equiaxed grain microstructure. In the normal direction to the build direction, the columnar grains are not aligned and are oriented randomly. On the other hand, equiaxed grains have a more isotropic microstructure, with grains randomly oriented in all directions. This leads to similar stiffness values in all directions.

One explanation of why columnar grains develops lower stiffness in the normal to build direction could be that the formation of columnar grains results in orientations mainly within <001> and <101> directions. The strongest crystal planes in <111> direction are not present due to the anisotropic nature. This phenomenon contributes to the reduced stiffness in the normal direction of the build direction compared to equiaxed grain microstructure. This is an important consideration when designing and using AM parts in applications where stiffness is a critical factor.

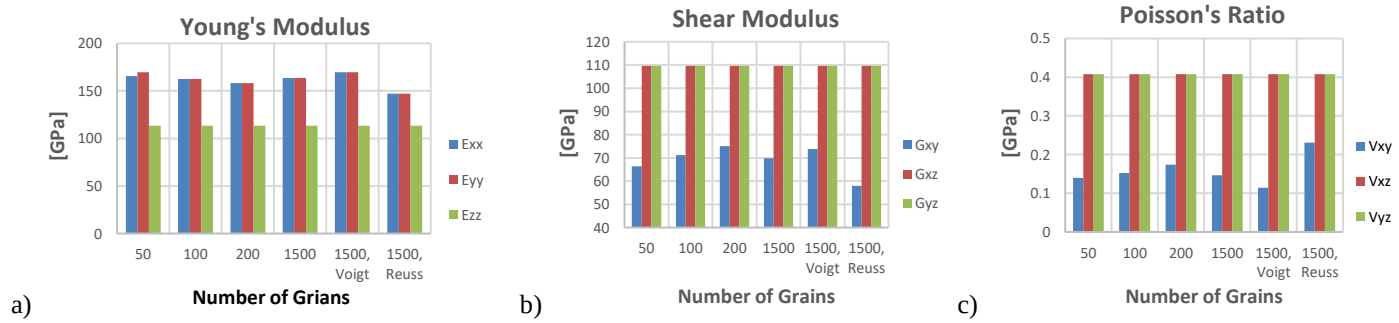

Fig. 3: Result summary of a) Young's modulus, b) shear modulus and c) Poisson's ratio.

By comparing the equiaxed and columnar RVE cases with the previously studies done, and the experimental data found in the literature, it can be noticed that the Young's modulus appears approximately at the same levels as others, see Fig. 4.

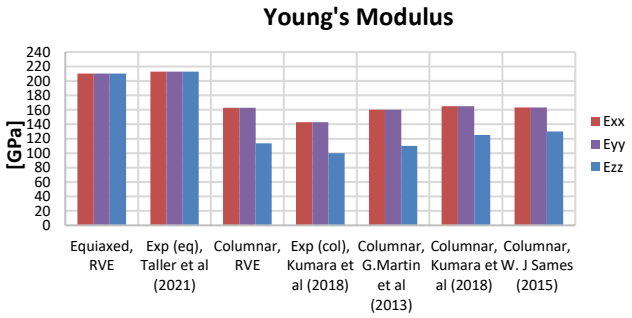

Fig. 4: Comparison studies and experiments done of Alloy 718 Young's modulus.

3.3. Combined Microstructure

The parameter which resulted in significant influence of the cohesive element, was the sharped shaped transition grains, see Fig.1. The sharp edges are not representing the reality which is of great importance to consider. Since these grains are automatically generated using Voronoi diagram and has the built-in function within Neper, it might be difficult to shape them differently. One way of how to eliminate them from the model is to apply the crop-function which cuts out the unwanted sharp grain corners. The crop-function has been applied to the cohesive element to minimize the numerical errors occurring during the virtual testing. The results showed some variety in homogenized stiffness levels seen in Fig.5 and the stiffness results show that this method might be applied for the transition zone modelling purpose. However, it needs explicit investigation and experimental validation to be concluded as valid. The results presented in Fig.5 seems reasonable since in the case T30 the sharp grain shapes have made a major effect on the homogenized stiffness in normal to build direction resulting in stiffness of 144 [GPa] while in the cases T20 and T15 the stiffness increases resulting in the stiffness of 150 [GPa] and 154 [GPa] respectively. The shear stiffness resulted in 37-39 [GPa] showing some minor variation.

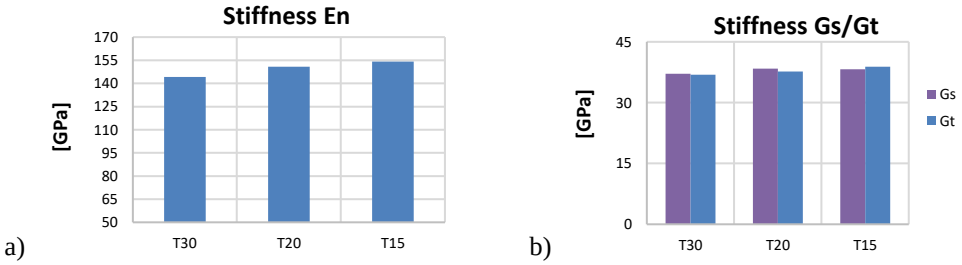

Fig. 5: Comparison summary of a) stiffness in normal to build direction and b) stiffness in shear directions.

The study of combined microstructure revealed local high stress concentrations at the interface area, see Fig.6. Here, von Mises stress distributions for tested 1500 equiaxed grain case are compared with the T15 combined case in the normal to the build direction. The columnar grain case results in a von Mises stress of 80.6 [MPa]. The reason for the high local stress distribution at the interface area of a combined microstructure, as compared to an equiaxed and columnar microstructure, can be attributed to stress concentrations due to the change of the microstructure properties. As a result, when a load is applied to the combined microstructure, the stresses are not uniformly distributed, but are concentrated in regions where the grains are oriented unfavourably with respect to the applied load. This can result in high stress concentrations at the interface area, which can lead to local plastic deformation, cracking, and even failure. In contrast, in an equiaxed microstructure, the grains are randomly oriented, resulting in a more homogeneous material response. This means that the stresses are more uniformly distributed, resulting in a lower stress concentration and a lower risk of failure. Overall, the anisotropic nature of the material in a combined microstructure leads to local stress concentrations at the interface area, which can be a limiting

factor for the mechanical performance of the material. Furthermore, the equivalent strain of 1500 equiaxed, columnar and T15 combined grain structures can be seen in Fig.6.

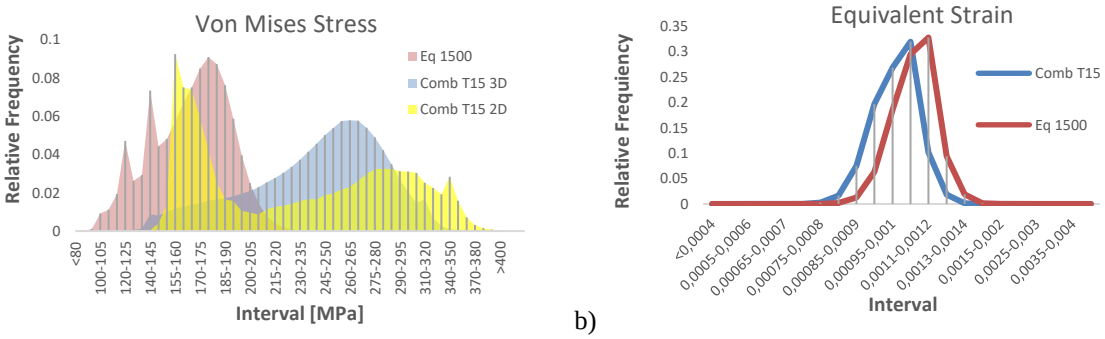

a) b)

Fig. 6: Comparison of a) Von Mises stress between 1500 equiaxed grain and combined T15 grain cases, and b) equivalent strain of 1500 equiaxed, columnar grains and T15 combined grain cases.

4. Conclusion

The work presented shows that the CEFE method can be applied for predictions of elastic anisotropic mechanical properties in superalloys that are produced via AM, by referring to the experimental work and other studies done previously. From this study, it is clearly shown that the elastic stiffness can be predicted for equiaxed and columnar microstructures accounting for their texture. The motivation for this study is that the CEFE method has not been explored fully when considering AM polycrystal materials. The interface of the grain morphological combinations shows significant changes in the elastic stiffness locally within the transition area which is also very important to consider when dealing with AM materials. This becomes even more important since the experimental stiffness measurements within the cohesive areas are very difficult at present. The application of the computational CEFE method shows promising results and might be used when studying not only stiffness of various grain morphologies but also the interface in the combined or hybrid AM microstructures. However, the combined microstructure models need additional further investigations where the RAE definition could be improved from the aspects of number of grains, the height of the RAE as well as the position of the transition interface area.

Acknowledgements

This work was financially supported by the PODFAM project and the PRIMUS Foundation. The Fundamental Research Funds for the University West.

References

[1] C. Körner, H. Helmer, A. Bauereiß, and R. F. Singer, “Tailoring the grain structure of IN718 during selective electron beam melting,” *MATEC Web Conf.*, vol. 14, 2014, doi: 10.1051/matecconf/20141408001.

[2] L. L. Parimi, G. Ravi, D. Clark, and M. M. Attallah, “Microstructural and texture development in direct laser fabricated IN718,” *Mater. Charact.*, vol. 89, pp. 102–111, 2014, doi: 10.1016/j.matchar.2013.12.012.

[3] A. Hinojos, J. Mireles, A. Reichardt, P. Frigola, P. Hosemann, L. E. Murr, R. B. Wicker, “Joining of Inconel 718 and 316 Stainless Steel using electron beam melting additive manufacturing technology,” *Mater. Des.*, vol. 94, pp. 17–27, 2016, doi: 10.1016/j.matdes.2016.01.041.

[4] M. M. Attallah, R. Jennings, X. Wang, and L. N. Carter, “Additive manufacturing of Ni-based superalloys: The outstanding issues,” *MRS Bull.*, vol. 41, no. 10, pp. 758–764, 2016, doi: 10.1557/mrs.2016.211.

[5] C. Kumara, D. Deng, J. Moverare, and P. Nylén, “Modelling of anisotropic elastic properties in alloy 718 built by electron beam melting,” *Mater. Sci. Technol. (United Kingdom)*, vol. 34, no. 5, pp. 529–537, 2018, doi: 10.1080/02670836.2018.1426258.

[6] H. Hu, “Elastic properties of cold-rolled and annealed sheets,” vol. 4, no. C, pp. 111–127, 1980.

[7] W. Hermann, H. G. Sockel, J. Han, and A. Bertram, “Elastic Properties and Determination of Elastic Constants of Nickel-Base Superalloys by a Free-Free Beam Technique,” no. January, pp. 229–238, 2012, doi: 10.7449/1996/superalloys_1996_229_238.
[8] Z. Wang, A. D. Stoica, D. Ma, and A. M. Beese, “Diffraction and single-crystal elastic constants of Inconel 625 at room and elevated temperatures determined by neutron diffraction,” *Mater. Sci. Eng. A*, vol. 674, pp. 406–412, 2016, doi: 10.1016/j.msea.2016.08.010.
[9] N. Kowalski, L. Delannay, P. Yan, and J. F. Remacle, “Finite element modeling of periodic polycrystalline aggregates with intergranular cracks,” *Int. J. Solids Struct.*, vol. 90, pp. 60–68, 2016, doi: 10.1016/j.ijsolstr.2016.04.010.
[10] M. H. Sia Nemat-Nasser, *Micromechanics: overall properties of heterogeneous materials*. .
[11] Í. Carneiro and S. Simões, “Recent advances in ebsd characterization of metals,” *Metals (Basel).*, vol. 10, no. 8, pp. 1–32, 2020, doi: 10.3390/met10081097.
[12] S. Ghorbanpour, M. E. Alam, N. C. Ferreri, A. Kumar, B. A. McWilliams, S. C. Vogel, J. Bicknell, I. J. Beyerlein, M. Knezevic, “Experimental characterization and crystal plasticity modeling of anisotropy, tension-compression asymmetry, and texture evolution of additively manufactured Inconel 718 at room and elevated temperatures,” *Int. J. Plast.*, vol. 125, no. September 2019, pp. 63–79, 2020, doi: 10.1016/j.ijplas.2019.09.002.
[13] L. Wang, M. Li, J. Almer, T. Bieler, and R. Barabash, “Microstructural characterization of polycrystalline materials by synchrotron X-rays,” *Front. Mater. Sci.*, vol. 7, no. 2, pp. 156–169, 2013, doi: 10.1007/s11706-013-0201-0.
[14] “MTEX.” https://mtex-toolbox.github.io/.
[15] “Neper.” https://neper.info/doc/index.html.
[16] “Dream 3D.” http://dream3d.bluequartz.net/.
[17] S. Ghosh and D. Dimiduk, *Computational methods for microstructure-property relationships*. 2011.
[18] G. Z. Voyiadjis and M. Yaghoobi, *Size Effects in Plasticity from Macro to Nano*. Elsevier, 2019.
[19] T. Ziegler, A. Neubrand, and R. Piat, “Multiscale homogenization models for the elastic behaviour of metal/ceramic composites with lamellar domains,” *Compos. Sci. Technol.*, vol. 70, no. 4, pp. 664–670, 2010, doi: 10.1016/j.compscitech.2009.12.022.
[20] Y. Tadano, M. Kuroda, and H. Noguchi, “Quantitative re-examination of Taylor model for FCC polycrystals,” *Comput. Mater. Sci.*, vol. 51, no. 1, pp. 290–302, 2012, doi: 10.1016/j.commatsci.2011.07.024.
[21] S. Tang and X. Zhu, “Clustering solver for displacement-based numerical homogenization,” *Theor. Appl. Mech. Lett.*, vol. 12, no. 3, p. 100306, 2022, doi: 10.1016/j.taml.2021.100306.
[22] “MATLAB.” https://ch.mathworks.com/products/matlab.html.
[23] S. Keshavarz and S. Ghosh, “Hierarchical crystal plasticity FE model for nickel-based superalloys: Sub-grain microstructures to polycrystalline aggregates,” *Int. J. Solids Struct.*, vol. 55, pp. 17–31, 2015, doi: 10.1016/j.ijsolstr.2014.03.037.
[24] J. Segurado, R. A. Lebensohn, and J. Llorca, “Computational Homogenization of Polycrystals,” *Adv. Appl. Mech.*, vol. 51, pp. 1–114, 2018, doi: 10.1016/bs.aams.2018.07.001.
[25] F. Roters, P. Eisenlohr, L. Hantcherli, D. D. Tjahjanto, T. R. Bieler, and D. Raabe, “Overview of constitutive laws, kinematics, homogenization and multiscale methods in crystal plasticity finite-element modeling: Theory, experiments, applications,” *Acta Mater.*, vol. 58, no. 4, pp. 1152–1211, 2010, doi: 10.1016/j.actamat.2009.10.058.
[26] J. Segurado, R. A. Lebensohn, and J. Llorca, “Computational Homogenization of Polycrystals,” *Adv. Appl. Mech.*, vol. 51, no. April, pp. 1–114, 2018, doi: 10.1016/bs.aams.2018.07.001.
[27] R. N. Saunders, A. Achuthan, A. P. Iliopoulos, J. G. Michopoulos, and A. Bagchi, “Effects of the Microstructural Grain Size and Aspect Ratio on the Mechanical Properties of Additively Manufactured Parts via Computational Analysis,” *Def. Tech. Inf. Cent.*, no. NRL/FR/6353--20-10,411, 2020.
[28] A. Lakshmanan, M. Yaghoobi, K. S. Stopka, and V. Sundararaghavan, “Crystal plasticity finite element modeling of grain size and morphology effects on yield strength and extreme value fatigue response,” *J. Mater. Res. Technol.*, vol. 19, pp. 3337–3354, 2022, doi: 10.1016/j.jmrt.2022.06.075.
[29] A. Aburakhia, A. Bonakdar, M. Molavi-Zarandi, J. Kelleher, and H. Abdolvand, “Deformation mechanisms of

additively manufactured Hastelloy-X: A neutron diffraction experiment and crystal plasticity finite element modeling," *Mater. Des.*, vol. 222, p. 111030, 2022, doi: 10.1016/j.matdes.2022.111030.
[30] P. W. Liu, Y. Z. Ji, Z. Wang, C. L. Qiu, A. A. Antonysamy, L.-Q. Chen, X. Y. Cui, L. Chen, "Investigation on evolution mechanisms of site-specific grain structures during metal additive manufacturing," *J. Mater. Process. Technol.*, vol. 257, no. October 2017, pp. 191–202, 2018, doi: 10.1016/j.jmatprotec.2018.02.042.
[31] I. Benedetti and F. Barbe, "Modelling Polycrystalline Materials: An Overview of Three-Dimensional Grain-Scale Mechanical Models," *J. Multiscale Model.*, vol. 05, no. 01, p. 1350002, 2013, doi: 10.1142/s1756973713500029.
[32] ABAQUS, "Abaqus 6.14," *Abaqus 6.14 Anal. User's Guid.*, p. 14, 2014.
[33] G. Martin, N. Ochoa, K. Saï, E. Hervé-Luanco, and G. Cailletaud, "A multiscale model for the elastoviscoplastic behavior of Directionally Solidified alloys: Application to FE structural computations," *Int. J. Solids Struct.*, vol. 51, no. 5, pp. 1175–1187, 2014, doi: 10.1016/j.ijsolstr.2013.12.013.
[34] K. K. Pathak, C. Namgyal, and S. Singh, "Effect of crystal structures on deformation behaviour of materials using finite element method," vol. 10, no. 4, 2014.